Journal of Applied Physics

Electronic properties of the $Zr-ZrO_2-SiO_2-Si(100)$ gate stack structure

Cite as: J. Appl. Phys. **99**, 063708 (2006); https://doi.org/10.1063/1.2181282
Submitted: 16 August 2005 • Accepted: 31 January 2006 • Published Online: 23 March 2006

C. C. Fulton, G. Lucovsky and R. J. Nemanich

View Online

Export Citation

ARTICLES YOU MAY BE INTERESTED IN

Band offsets of wide-band-gap oxides and implications for future electronic devices
Journal of Vacuum Science & Technology B: Microelectronics and Nanometer Structures Processing, Measurement, and Phenomena **18**, 1785 (2000); https://doi.org/10.1116/1.591472

Measurement of the band offsets of SiO_2 on clean n- and p-type GaN(0001)
Journal of Applied Physics **93**, 3995 (2003); https://doi.org/10.1063/1.1559424

High-κ gate dielectrics: Current status and materials properties considerations
Journal of Applied Physics **89**, 5243 (2001); https://doi.org/10.1063/1.1361065

Challenge us.
What are your needs for periodic signal detection?

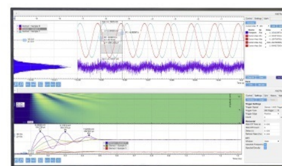

Zurich Instruments

© 2006 American Institute of Physics.

Electronic properties of the $Zr-ZrO_2-SiO_2-Si(100)$ gate stack structure

C. C. Fulton, G. Lucovsky, and R. J. Nemanich[a)]
Department of Materials Science and Engineering, and Department of Physics, North Carolina State University, Raleigh, North Carolina 27695-8202

(Received 16 August 2005; accepted 31 January 2006; published online 23 March 2006)

The interface electronic structure of a layered $Zr-ZrO_2-SiO_2-Si(100)$ system was studied with x-ray ($h\nu = 1254$ eV) and ultraviolet ($h\nu = 21.2$ eV) photoemission spectroscopies. *In situ* growth and characterization allow the structures to be deposited and studied in a stepwise manner without the risk of contamination. This study discusses the electronic properties including electron affinities and work functions, valence band maxima, band bending in the Si, and internal fields in a layered high-κ gate stack. With this information the band alignments can be reconstructed and compared to predictions of the vacuum alignment models (i.e., the Schottky-Mott model for metal-semiconductor interfaces or the electron affinity model for heterojunctions) and the interface induced gap states model. The vacuum alignment models are first order approaches to determine the electronic barrier height for a heterojunction, and interface bonding can contribute to charge transfer across the interface, affecting the dipole contribution and altering the barrier heights. In this study, the band offsets and vacuum levels are independently measured, thereby determining the deviation from the vacuum level alignment models. The valence band offsets at the $Si-SiO_2$, SiO_2-ZrO_2, and ZrO_2-Zr are found to be 4.4 ± 0.1, 0.67 ± 0.24, and 4.9 ± 0.44 eV, respectively. For these same interfaces the deviations from the electron affinity or Schottky-Mott model are determined to be 0.2 ± 0.14, -1.43 ± 0.29, and 1.3 ± 0.39 eV, respectively. © *2006 American Institute of Physics*.
[DOI: 10.1063/1.2181282]

I. INTRODUCTION

The planned scaling of integrated circuit devices involves a reduction of the gate insulator thickness to obtain the targeted capacitance and sheet charge density in the channel. As the gate dielectric thickness is reduced below 2 nm, direct tunneling between the gate and channel becomes significant, leading to increased power consumption. As an alternative to reducing the physical thickness of the gate oxide, the dielectric constant could be increased. This would allow the desired increase in capacitance with a physically thicker layer, resulting in both a reduced tunneling current and an increase in sheet charge density. With devices based on conventional silicon oxides and oxynitrides approaching their physical limits, the exploration of alternative materials has gained significant momentum.[1]

The fundamental criteria for a gate dielectric include barrier heights that will effectively block both electrons and holes, chemical stability in contact with both the silicon substrate and the gate material, and a low density of interface electronic states. Zirconium oxide, with its large band gap of ~5.7 eV and dielectric constant of ~25, is of particular interest as a gate dielectric.[1–3] Moreover, the ZrO_2-Si band offsets have been predicted to be favorable for blocking both holes and electrons.[4]

Integrating a transition metal (TM) oxide in place of SiO_2 is a complex process. The deposition of TM oxides on Si often results in an interfacial SiO_x layer which, although it can lower the interface state density and improve device characteristics, must be carefully controlled as it has a much lower dielectric constant than the TM oxide and can significantly limit the minimum achievable effective oxide thickness (EOT). It is also desirable to replace the heavily doped poly-Si with a metal as the gate material. While poly-Si can be appropriately doped for both *n*- and *p*-type devices, it still exhibits a significant depletion width to terminate the field applied to the device gate. This depletion width also contributes to the total EOT in a device, and replacing the poly-Si with a metal with a much shorter depletion width becomes necessary for aggressively scaled devices.[5] Any metal to be used as a gate material must be chemically stable when in contact with a TM oxide. Additionally, the metal and its characteristic work function must be chosen appropriately for *n*- and *p*-type devices. Thus, the integration of high-κ dielectric materials into a device is a much more complex process than that for a thermal oxide or even a deposited oxynitride.

The internal interfaces of the gate stack will significantly affect the performance of the devices. Chemical bonding occurs at these interfaces, and the charge transfer across these bonds can result in an interface dipole.[4,6] In addition, dangling bonds and defects at the interface can contribute to this charge transfer, which may lead to internal fields in the gate stack. The Schottky-Mott model for metal-semiconductor junctions and, by extension, the electron affinity model for semiconductor-semiconductor junctions are based on the alignment of the vacuum level of the two materials.[7] While it is evident that these models are based on a highly idealized interface, the advantage is that the barrier heights and band offsets can be estimated from measurable quantities (i.e., work functions and/or electron affinities). Alternatively, the band alignment has been described with nonspecific heuristic

[a)]Electronic mail: robert_nemanich@ncsu.edu

 © 2006 American Institute of Physics

approaches such as the charge neutrality model discussed extensively by Robertson,[4] Peacock and Robertson,[8] and Mönch.[9]

The vacuum level alignment models presume that the bonding across the interface does not significantly affect the surface electronic states on each material which determine the work function of those materials. In essence, the potential difference between the values predicted by the vacuum level alignment models and the observed interface band alignment represents the change in the interface dipole due to the interface formation. Similarly, the difference in the vacuum alignment models and the charge neutrality model represents a theoretical prediction of the change in the interface dipole. This change in the interface dipole is related to the polarity of the interface bonding and the net charge transfer across that interface.

In this research *in situ* photoelectron spectroscopy has been employed to directly and independently measure the band alignment at each interface in the gate stack structure. The techniques allow a direct measurement of the valence band offsets for semiconducting and/or dielectric layers. While for metal-dielectric interfaces, the techniques will determine the offset between the metal Fermi level and the dielectric valence band.

In order to determine the change of the dipole at each interface, it is necessary to determine the metal work function and/or the electron affinity of the dielectric or semiconductor. For semiconductors and dielectrics, the determination of the electron affinity requires knowledge of the band gap. An independent measurement of the valence band maximum and the vacuum level of each material at an interface allows an expression of the conduction band offset (CBO) as the difference in electron affinities plus an additional term that is ascribed to the contribution from the interface dipole $[\phi_{\text{CBO}}=(\chi_1-\chi_2)\pm\Delta]$. This additional term Δ can either increase or decrease the band offset depending on the specific chemistry at the interface in question. Similarly for a metal-semiconductor (or a metal-dielectric) interface, the contact potential as defined by the Schottky-Mott model will also be corrected with an additional term to accommodate the contribution from the interface dipole $[\phi_{\text{bh}}=(\Phi_M-\chi)\pm\Delta]$. Where ϕ_{bh} is the conduction band barrier height, Φ_M is the metal work function, and χ is the semiconductor or oxide electron affinity. In the experiments presented here, all values are measured and only the band gap of the semiconductor or dielectric is required to determine the conduction band alignment.

The basic approaches of these studies are to employ *in situ* deposition and characterization to fabricate thin film structures that approximate a gate stack and to use photoemission to characterize the development of the electronic properties in a stepwise manner. Through the combined x-ray and ultraviolet photoemission measurements we are able to determine the band alignment, the metal work functions, and the electron affinities in each layer as well as the band bending to the Si substrate and the presence of internal fields in the dielectric layers. By comparison with the appropriate Schottky-Mott and electron affinity models, the change of the interface dipole can be deduced for each interface.

II. EXPERIMENT

All experiments were performed on 25 mm diameter, n-type, 0.05–0.1 Ω cm (3×10^{18} to 1×10^{17} cm^{-3} phosphorus), Si(100) wafers. These wafers were loaded into an UHV integrated growth and analysis system which includes a linear UHV transfer system interconnecting 16 different process and characterization chambers. Four of these chambers were employed in this study for steps including plasma oxidation, reactive deposition of ZrO_2, electron beam deposition of Zr metal, x-ray photoemission spectroscopy (XPS), and ultraviolet photoemission spectroscopy (UPS).

An initial oxygen plasma exposure was employed to remove residual hydrocarbon contamination and to form the thin (0.5 nm) oxide buffer layer. Zirconium oxide thin films were grown by electron beam evaporation of zirconium metal in an O_2 ambient followed by a 30 s remote oxygen plasma exposure to ensure complete oxidation. The samples were then *in situ* annealed to 500 °C for 5 min to achieve a stable state.[10,11] Metal layers were electron beam evaporated in vacuum. After each process step the films were analyzed with XPS and UPS to observe trends in the electronic properties.

Formation of the initial SiO_2 buffer layer and the post-high-κ oxidation step were performed in a remote plasma-enhanced chemical vapor deposition (RPECVD) chamber with a base pressure of 5×10^{-9} Torr. Remote plasma exposures took place with the sample at room temperature, with a gas flow of 10 SCCM (SCCM denotes cubic centimeter per minute at STP) of O_2 and 50 SCCM of He and an operating pressure of 60 mTorr. To minimize ion damage from the plasma the substrate is located ~20 cm downstream of the discharge region in which the plasma was excited by 20 W rf power.

The zirconium oxide was deposited with the substrate at room temperature in an UHV chamber with a base pressure of 8×10^{-10} Torr by electron beam evaporation of Zr metal at a rate of ~0.05 nm/s (measured by a quartz crystal oscillator) in an ambient of 2×10^{-6} Torr O_2. The pressure of research-grade O_2 was regulated using a precision leak valve and a turbomolecular pump (TMP). Following the oxide deposition, samples were exposed to a remote oxygen plasma (same conditions and time as used for the initial buffer layer) and vacuum annealed to 500 °C for 5 min.

The approximate oxide film thickness can be deduced from the thickness of the deposited metal layer using the molar densities and the molar masses of the TM and its oxide. This analysis gives a ratio of 1.5:1 for the thickness of a ZrO_2 film formed from Zr metal. The estimated film thicknesses discussed here are calculated accordingly and assume complete oxidation of the deposited TM layer. A second method for determining the thickness of thin films by XPS has been described by Shallenberger *et al.*[12] The molar density thicknesses were corroborated by the relative intensity changes of the Si bulk peak from the Si 2p core level spectra, as a function of film thickness.

In this research, ultraviolet photoemission spectra were obtained using a He discharge lamp primarily generating the He I line at 21.2 eV in a chamber with an operating pressure

of 3×10^{-9} Torr. A VSW 50 mm mean radius hemispherical analyzer and VSW HAC300 were operated with a pass energy of 10 eV, resulting in an electron energy resolution of 0.1 eV. A negative 4.00 V bias was applied to the sample to assure that the photoelectrons can overcome the analyzer work function. All photoemission spectra are presented in binding energy relative to the system Fermi level, and the electron spectrometer has been calibrated by defining the Fermi edge of an *in situ* deposited Au film as zero binding energy.

Ultraviolet photoemission spectroscopy probes to a depth of 0.5–1.0 nm. Features in the spectrum are a reflection of the valence band density of states. The valence band maximum (VBM) can be determined with respect to the system Fermi level which will correspond to the Fermi level in the bulk of the Si. Since the band bending and internal fields can be determined from XPS, then the actual valence band offset (VBO) can be determined for the uppermost layer with respect to the lower layers and the Si VBM. The high binding energy cutoff of the valence band spectrum represents the vacuum level at the surface. The vacuum level with respect to the Fermi level (i.e., the work function) is determined from the photon energy minus the binding energy of the vacuum cutoff. For the case of a semiconductor or dielectric layer, the conduction band position and the electron affinity can be determined with knowledge of the band gap.

X-ray photoemission spectra were obtained at a pressure of 2×10^{-9} Torr using the 1253.6 eV Mg $K\alpha$ or the 1486.6 eV Al $K\alpha$ line from a VG Microtech (now Thermo Electron Corp) XR3 dual anode source and a VG Microtech Clam II electron analyzer. The resolution of the analyzer was determined from the full width at half maximum (FWHM) of a gold $4f$ 7/2 spectral peak to be approximately 1.0 eV; however, through curve fitting, the centroid of spectral peaks can be resolved to ±0.1 eV. The Fermi level of the analyzer was obtained from the measured binding energy of the gold $4f$ 7/2 peak position which is calibrated to 84.0 eV. Observation windows were set around the Si $2p$, O $1s$, and Zr $3d$ core level binding energies to record shifts.

For gate structures limited to a total thickness of ~4 nm, x-ray photoemission can probe the entire gate stack including the silicon substrate. Since the depletion width of moderately doped (~10^{17} cm^{-3}) Si is much greater than the sampling depth of XPS, we can assume that the Si $2p$ XPS core level associated with the Si substrate indicates the binding energy of states at the Si-dielectric interface. Thus, changes in the binding energy of this feature will accurately indicate changes in the band bending in the Si. Additionally, changes in the Si band bending are typically associated with the development of an internal field in the dielectric.

As layers are added to the gate stack, spectroscopic shifts are observed in the core level spectra of the underlying dielectric, which can be attributed to a field in the oxide. If there is an internal field in the layer, the potential of the atoms will change across the thickness of the films and the binding energy detected in the XPS core levels will be shifted to reflect this change. For a thin layer the presence of a field would result in the XPS peak to be shifted by an amount equal to one-half of the potential change across the layer. Here we assume that the x-rays excite photoemission uniformly across the layer, the photoelectrons are not attenuated, and the potential changes linearly across the layer. In this case the spectral centroid will correspond to the binding energy of the atoms at the center of the layer. For example, for a SiO_2 layer with an internal field that would result in a 1 V change in potential we would expect the centroid of the core level peaks to be shifted by 0.5 eV, an amount representative of the potential at the center of the film.

While uniform excitation from the x-ray source is a reasonable approximation, the probability of a photoelectron escaping the layer depends exponentially on the depth from which the photoelectron was emitted. Consequently, the observed core level spectrum becomes the weighted average of the photoemission from all atoms between the two interfaces of the layer. Thus, if a potential exists across a layer, then the centroid position of the core level spectrum will reflect the potential at a position displaced from the center of the layer towards the outer surface.

The following describes our approach to account for this effect and to determine the total potential across a given layer from the measured shift of a core level peak. We assume that the layer thickness and the photoelectron attenuation are known. The photoelectron signal intensity, I, will be attenuated for increased depths in the film. The intensity from any thickness is given by

$$I = I_0 e^{-z/\lambda}, \tag{1}$$

where I_0 is the signal intensity for the atoms at the surface, z is the depth from which the photoelectron originates, and λ is the photoelectron inelastic mean free path. The electron mean free path is an energy-dependent function that has been approximated by a power law expression $\lambda = kE^p$.[13] Ashley and Tung have tabulated data for the parameters k and p (both experiment and theory) for electron energies that are in the range considered here (400–2000 eV).[14] The electron inelastic mean free path in a SiO_2 film for an electron kinetic energy of 1150 eV (i.e., Si $2p$ core level) is found to be ~3.2 nm ($k=0.218$ and $p=0.706$).

Assuming that λ is constant in the energy range over which the core level spectra are observed to shift (~1 eV) we can then determine the depth, Z_{av}, that will represent the centroid binding energy of the observed photoelectron spectrum which is given by

$$Z_{av} = \frac{\int_{z_1}^{0} f(z)w(z)dz}{\int_{z_1}^{0} w(z)dz}, \tag{2}$$

where z_1 is the thickness of the layer, and the functions $f(z)$ and $g(z)$ are of the form

$$f(z) = z \text{ and } w(z) = e^{-z/\lambda}. \tag{3}$$

Substituting the values appropriate for the Si $2p$ core level peak from Ashley and Tung and the calculated electron mean free path into Eq. (2), the weighted average depth is then given by

TABLE I. XPS peak positions and UPS valence band features after each deposition step. The values are in binding energy (eV) relative to the Si E_F with an error of ±0.1 eV

Process step	0.5 nm SiO_2	1.0 nm ZrO_2	1.0 nm Zr
Si 2p (Bulk)	99.6	99.6	99.8
Si 2p (SiO_2)	103.3	103.1	103.6
Zr 3d (ZrO_2)	n/a	183.0	183.3
Zr 3d (metal)	n/a	n/a	179.4
VBM	5.2	4.2	0.0
E_{vuc}	16.6	17.7	17.1

$$Z_{\text{av}} = \frac{3.2[1 - e^{-z_1/3.2}(z_1/3.2 + 1)]}{1 - e^{-z_1/3.2}}, \tag{4}$$

where z_1 is the thickness of the layer in nanometers and 3.2 is the calculated electron mean free path, also in nanometers.

The observed centroid of the core level spectrum corresponds to the binding energy of a photoelectron emitted from a depth of Z_{av}; thus, if there exists a potential across a layer from which photoelectrons are extracted then the centroid of the core level spectrum will be shifted in energy by the potential at the depth Z_{av}. For example, if SiO_2 layer is 1.0 nm thick then Eq. (4) indicates that the Z_{av}=0.4 nm, and if the potential across the layer is 1.0 V then the observed spectral centroid would be shifted 0.6 eV from the zero potential condition. The observed shift is related to the total potential across the layer by

$$V_{\text{tot}} = \frac{V_{\text{obs}}}{1 - Z_{\text{av}}} = \frac{0.6\text{ V}}{1 - 0.4} = 1.0\text{ V}. \tag{5}$$

We deduce that an observed shift of 0.6 eV in a 1.0 nm thick layer corresponds to a total potential across the layer of 1.0 V. In this way, it is possible to correlate the observed core level shift from a thin film of known thickness to the total potential across the layer.

III. RESULTS

With stepwise growth and *in situ* characterization, changes in the electronic structure can be observed layer by layer as the gate stack structure is formed. In the following sections the results are described from each layer in the structure beginning with the 0.5 nm SiO_2 buffer layer. A summary of the experimental results is presented in Table I.

A. 0.5 nm SiO_2

Figure 1 presents the XPS Si 2p core level spectrum for 0.5 nm SiO_2 on n-Si. Fitting of the Si 2p spectral features indicates the substrate-related feature at a binding energy of 99.6 eV and the Si–O bonded feature from the SiO_2 buffer layer at 103.3 eV.

Ultraviolet photoemission spectroscopy yields a plot which reflects features of the total density of states of the SiO_2 valence band. As in all of the photoemission spectra the zero energy reference is the bulk Fermi level of the system. Figure 2 shows the valence band spectrum for 0.5 nm SiO_2 on n-Si. The lower binding energy (front) edge of the spectrum represents the VBM and the higher binding energy (back) edge represents the vacuum level. By fitting the front of the spectrum (using a linear fit through the point of maximum slope), we find that the VBM of the SiO_2 is 5.2 eV with respect to the substrate Fermi level. Fitting of the vacuum cutoff is completed in a similar way. The data indicate the vacuum cutoff at 16.6 eV below E_F.

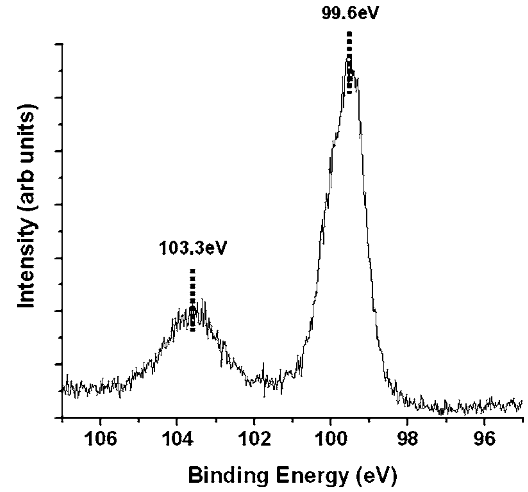

FIG. 1. The Si 2p XPS core level spectra of 0.5 nm SiO_2 on n-Si(100). The feature at 99.6 eV shows Si–Si bonding that is attributed to Si in the substrate and the feature at 103.3 eV is attributed to Si–O bonding in SiO_2.

B. 1.0 nm ZrO_2

In situ XPS and UPS measurements are repeated after deposition of 1.0 nm ZrO_2 (Figs. 3 and 4). Shifts in the bulk Si 2p core level (~99 eV) are ascribed to changes in the Si substrate band bending, and shifts in the oxide-bonded Si 2p core level (~103 eV) from the interfacial SiO_2 indicate a field in the oxide. Figure 3 shows the Si 2p core level spectrum both before and after ZrO_2 deposition. With deposition of the high-κ material the core level position for Si in the substrate is unchanged at 99.6 eV (to within the experimental error of ±0.1 eV), and with the deposition of the high-κ material, the SiO_2 related peak is shifted 0.2 eV lower in binding energy to 103.1 eV. A spectrum was also obtained

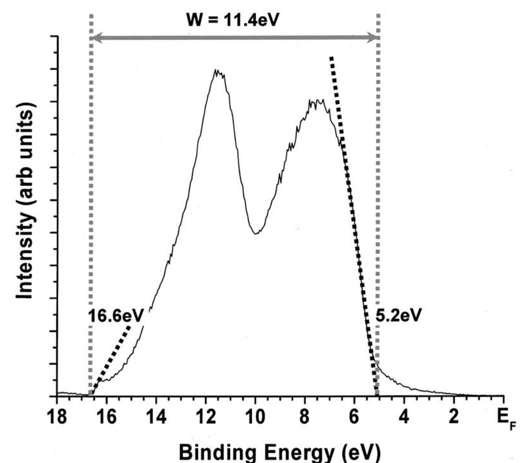

FIG. 2. The UPS valence band spectrum of 0.5 nm SiO_2 on n-Si. The VBM (5.2 eV) and the cutoff due to the vacuum level (16.6 eV) are indicated.

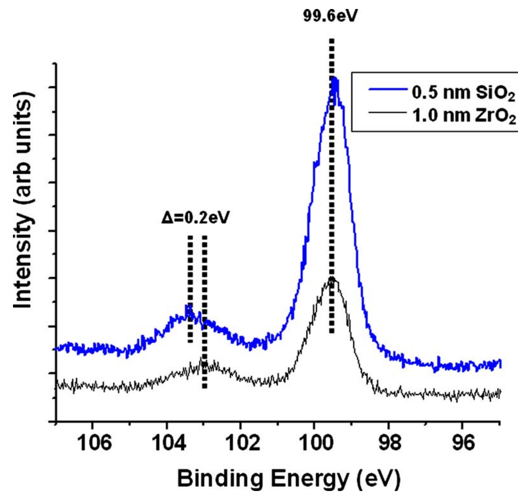

FIG. 3. (Color online) The Si 2p XPS core level spectra before (blue) and after (black) deposition of 1.0 nm ZrO_2. After deposition the substrate related peak is unchanged and the oxide related peak is shifted 0.2 eV lower in binding energy.

for the Zr 3d doublet core level which indicated a Zr 3d 5/2 peak at a binding energy of 183.0 eV.

Ultraviolet photoemission probes only the topmost layer (ZrO_2 in this case) and the scan shown in Fig. 4 indicates the features of the valence band total density of states versus binding energy. Fitting the VBM and vacuum level as shown in Fig. 4, the two features are found at 4.2 and 17.7 eV, respectively.

C. 1.0 nm Zr metal

Shifts are observed in the core level peaks with the deposition of 1.0 nm of Zr onto the oxide gate stack. The Si 2p core level again gives insight into band bending and the field in the SiO_2 layer. After Zr deposition the Si substrate core level (Fig. 5) is shifted 0.2 eV higher in binding energy (to 99.8 eV), indicating a downward change in band bending of 0.2 eV. The Si core level from SiO_2 shows a larger 0.5 eV shift to a higher binding energy of 103.6 eV. This shift is opposite in direction when compared to the shift observed with ZrO_2 deposition and again indicates a field in the SiO_2 but one with an opposite sign.

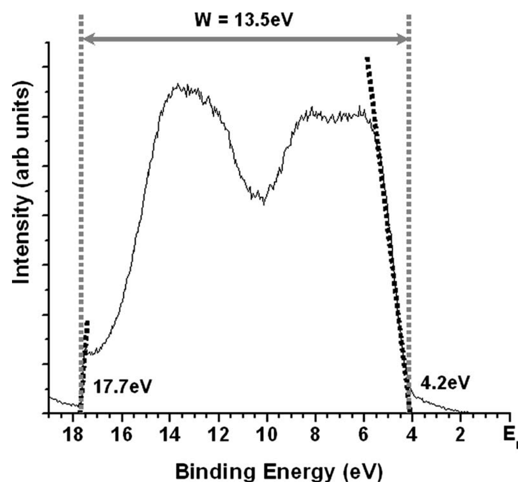

FIG. 4. The UPS valence band spectrum of 1.0 nm ZrO_2. The VBM (4.2 eV) and the vacuum level (17.7 eV) are indicated.

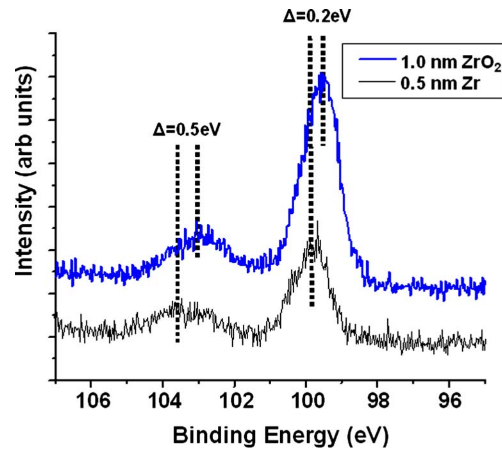

FIG. 5. (Color online) The Si 2p XPS core level spectra before (blue) and after (black) deposition of 1.0 nm Zr. After deposition the substrate related peak is shifted 0.2 eV higher in binding energy and the oxide related peak is shifted 0.5 eV lower in binding energy.

The Zr 3d core level doublet (Fig. 6) can be used to obtain information about the field in the ZrO_2 layer. The core levels of Zr metal and ZrO_2 overlap somewhat and require a deconvolution to separate the contributions from oxide related (higher binding energy) from the metal related (lower binding energy) peaks. The deconvoluted oxide related Zr 3d core level indicated a shift to higher binding energy of 0.3 eV (to 183.3 eV) when compared to the deposited ZrO_2.

Valence band spectra of metallic films display emission that extends to the Fermi level of the system (zero binding energy), as shown in Fig. 7. The vacuum level cutoff of the Zr metal spectrum is found to be 17.1 eV.

IV. DISCUSSION

We now discuss the results from each layer in the structure beginning with the 0.5 nm SiO_2 buffer layer and apply

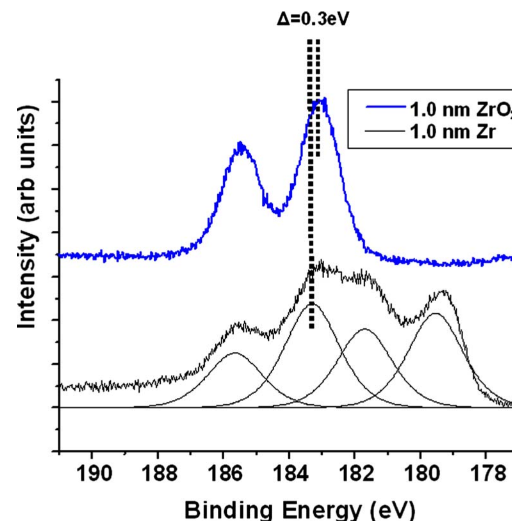

FIG. 6. (Color online) The Zr 3d XPS core level spectra before (blue) and after (black) deposition of 1.0 nm Zr metal. After deposition the oxide related 3d 5/2 peak is shifted 0.3 eV higher in binding energy.

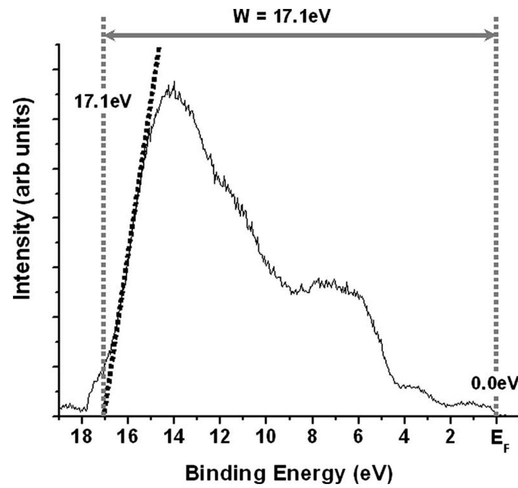

FIG. 7. The UPS valence band spectrum after deposition of 1.0 nm of Zr on ZrO_2. The emission extends to the Fermi level, indicating metallic character, and the vacuum cutoff is observed at 17.1 eV.

the analysis that was described above to determine the band offsets, internal fields, and interface dipoles. A summary of the deduced results is presented in Table II.

A. 0.5 nm SiO_2

In an effort to determine the band bending of the initial oxidized surface, we had previously measured the VBM and Si 2*p* core level of a clean, hydrogen-terminated Si(100) surface.[15] For a wafer of the same specification as those used in this study, we find the Si VBM to be 0.8 eV below the Fermi level, and the Si 2*p* core level at 99.6 eV. This results in an energy difference between the Si 2*p* core level and the VBM of $\Delta E = 98.8 \pm 0.1$ eV, a value similar to that of other reports.[16,17]

From the study noted above and our measurement of the Si 2*p* bulk core level at 99.6 eV below the Si E_F, we determine that the Si VBM is 0.8 eV below E_F or that the Fermi level is 0.3 eV below the Si conduction band maximum (CBM). This is a reasonable value (within ±0.1 eV) for *n*-type Si doped to the mid-10^{17} cm^{-3} range. The results indicate that to within the measurement error of ±0.1 eV the Si underlying the 0.5 nm SiO_2 interface layer has flat bands.

TABLE II. Tabulated electronic structure for the $Si-SiO_2-ZrO_2-Zr$ system including band bending, internal potentials, VBOs, electron affinities, and the deduced change in the interface dipole. The VBO includes band bending and internal fields. The conduction band offset (CBO) assumes a band gap (9.0 eV for SiO_2 and 5.7 eV for ZrO_2). The values are ±0.1 eV.

Process step	0.5 nm SiO_2	1.0 nm ZrO_2	1.0 nm Zr
Band bending	0.0±0.1	0.0±0.1	0.2±0.1
Potential (SiO_2)	n/a	−0.33±0.17	0.17±0.17
Potential (ZrO_2)	n/a	n/a	0.0±0.1
VBO (wrt Si)	4.4±0.1	3.73±0.19	n/a
CBO (wrt Si)	3.5±0.1	0.87±0.19	n/a
χ/Φ_M	0.8±0.14	2.0±0.14	4.1±0.14
Dipole (Δ)	0.2±0.14	−1.43±0.29	1.3±0.39

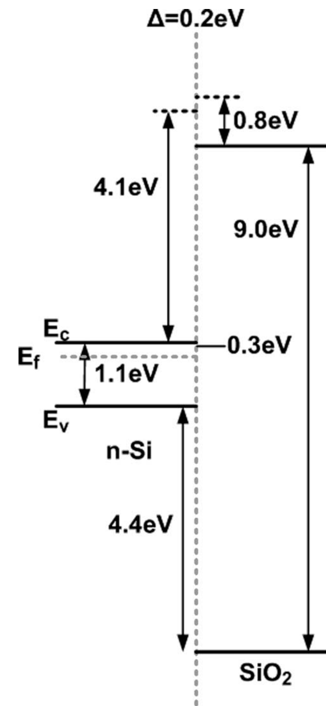

FIG. 8. A schematic band diagram for 0.5 nm SiO_2 on *n*-Si. The band offsets and electron affinities are indicated and a change in the interface dipole of $\Delta = 0.2$ eV is deduced.

From the UPS measured position of the oxide VBM and the knowledge of the Fermi level position within the Si gap, the VBO for a 0.5 nm SiO_2 film on Si is determined to be 4.4±0.1 eV (VBO=5.2±0.1−0.8=4.4±0.1 eV).

The electron affinity of the SiO_2 buffer is determined from the photon energy used to excite the valence band spectrum (21.2 eV), the measured width of the UPS spectrum (i.e., the vacuum level—VBM), and the reported band gap (9.0 eV). The electron affinity is determined from the expression $\chi = h\nu - W - E_g$. In this case, using a band gap for SiO_2 of 9.0 eV we find that $\chi = 21.2 - 11.4 \pm 0.14 - 9.0 = 0.8 \pm 0.14$ eV. Determining the electron affinity requires knowledge of the band gap which has not been measured in this study and is taken from literature sources. Consequently, the electron affinities reported will vary with the particular literature value for the dielectric band gap.

With the band bending information from XPS, the deduced VBO, and the electron affinity, a schematic band diagram can be constructed (Fig. 8). Note that the VBO is determined independently from the vacuum level. In these experiments the Si vacuum level has not been measured and the electron affinity of 4.1 eV is from the literature, as are the values for the oxide band gaps.[18] In these measurements the alignment of the vacuum levels has been determined independently and the deviation from the electron affinity rule, that is, the difference in vacuum levels of the two materials, is then ascribed to the change of the interface dipole. In this case the deviation is $\Delta = 0.2 \pm 0.14$ eV. For SiO_2 on Si the dipole change effectively increases the barrier for electrons in the Si conduction band.

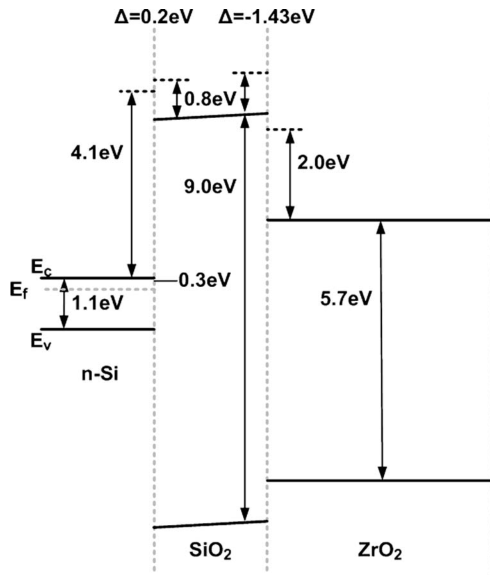

FIG. 9. A schematic band diagram for 1.0 nm ZrO_2 on 0.5 nm SiO_2 on n-Si. The band offsets and electron affinities are indicated as are the change of the interface dipole and the presence of a field in the SiO_2 layer.

B. 1.0 nm ZrO_2

Following the ZrO_2 deposition, the binding energy of the Si 2p substrate core level position is unchanged; from this we conclude that, to within ±0.1 eV, the Si bands are flat as they were with the 0.5 nm SiO_2 layer. Using Eq. (4) with $z_1=0.5$ nm, we find that the centroid of the shifted SiO_2 feature is representative of the field at a depth of 0.2 nm. When corrected for the exponential dependence of the electron escape probability, we find that the 0.2±0.1 eV shift in the SiO_2 related Si 2p core level corresponds to a 0.33±0.17 V potential across the SiO_2 layer. This analysis is dependent on the deduced value of the SiO_2 thickness; however, the correction is relatively insensitive. For example, if the SiO_2 thickness was 1 nm (instead of the deduced 0.5 nm), the analysis based on the measured 0.2 eV shift would indicate a potential across the film of 0.26 V.

A potential across the SiO_2 layer can alter the observed band offset for ZrO_2 with respect to the Si E_F. Therefore, the VBO of the ZrO_2 relative to the Si VBM can then be corrected to a zero potential case, and we find that the VBO $=4.2\pm0.1-0.8+0.33\pm0.17=3.73\pm0.19$ eV. Using the same procedure as described above for SiO_2 the electron affinity of ZrO_2 is found to be $\chi=21.2-13.5\pm0.14-5.7=2.0\pm0.14$ eV where the band gap was assumed to be 5.7 eV. After the interface has formed the valence band offset of the ZrO_2 on SiO_2 is found to be 0.67±0.24 eV where the large fractional error arises because the measurement involves the differences of three measurements.

With the information gained from the XPS and UPS measurements the schematic band diagram can be constructed which now includes the 1.0 nm ZrO_2 layer (Fig. 9). The band offset has been determined independently of the electron affinities.

The change of the interface dipole is deduced from the measured valence band offset and the measured position of the vacuum level (VL) of the SiO_2 relative to the SiO_2 VBM and the ZrO_2 relative to the ZrO_2 VBM. The VL of each dielectric layer is determined from the width of the UPS spectrum (W) using the expression $\text{VL}=h\nu-W$. For SiO_2 the vacuum level is found to be 9.8 eV above the VBM, and for ZrO_2 the vacuum level is found to be 7.7 eV. The change of the interface dipole, determined from $\Delta=[\text{VL}(ZrO_2)+\text{VBO}]-\text{VL}(SiO_2)$ is then $\Delta=-1.43\pm0.29$ eV.

The field in the SiO_2 layer and the measured flat bands may seem inconsistent; however, the band bending would be at or near to the 0.1 eV experimental uncertainty. In fact, in other measurements of ZrO_2 on 0.5 nm SiO_2 on different Si substrates, we have detected band bending ~0.1 eV, but this again is at the limits of the experimental uncertainty. The results shown here are from a single experiment and are not an average of multiple data sets.

Miyazaki *et al.* have published results for the system of ZrO_2-SiO_2-Si(100) which was grown by the alternative method of oxygen annealing a deposited ZrO_2 film on Si to grow a subcutaneous SiO_2 layer.[19] They have reported that this method leads to the incorporation of a few at. % Zr in the layer. Their published VBO with respect to Si for the subcutaneous SiO_2 is 4.35 eV, slightly lower than our measured 4.4 eV. The band offset reported for ZrO_2 on SiO_2 of 1.2 eV is larger than our result of 0.67 eV. When the method of growth is considered it is probable that the composition of the interfacial layer is different from our remote plasma grown films. Therefore, the interfaces may not be as well defined and a composition gradient may exist distorting the perceived valence band offset.

C. 1.0 nm Zr metal

After deposition of the Zr layer the SiO_2 related component of the Si 2p core level spectra is shifted 0.5±0.1 eV higher in binding energy. However, previously the shift after deposition of ZrO_2 was 0.2±0.1 eV to lower binding energy. The net change is then 0.3±0.1 eV from the initial (SiO_2 buffer layer) flat band condition.

In this analysis we are assuming a stacked structure $Zr-ZrO_2-SiO_2-$Si where the layers are well defined and their interaction is localized at the interfaces. In keeping with this layered model the interpretation of the core level shifts must take into consideration the shifts of each underlying layer. For instance, if the Si substrate core level is shifted 0.2±0.1 eV due to band bending and the SiO_2 layer on top is shifted 0.3 eV then this is a net observed shift of the SiO_2 layer of 0.1±0.1 eV. This net shift of 0.1 eV in the SiO_2 Si 2p core level can then be used to determine the total potential across the SiO_2 layer, where we find it to be 0.17±0.17 V.

To determine the potential across the ZrO_2 layer we must first consider the contribution from the band bending and the potential across the SiO_2. The band bending was determined to be 0.2±0.1 eV, and the potential across the SiO_2 layer was found to be 0.17±0.17 V, which results in a total shift due to the underlying layers of 0.37±0.19 eV. Thus, the potential across the high-κ layer is less than the experimental error of ±0.19 eV and the entire shift in the electronic structure can be ascribed to the band bending and the potentials in the

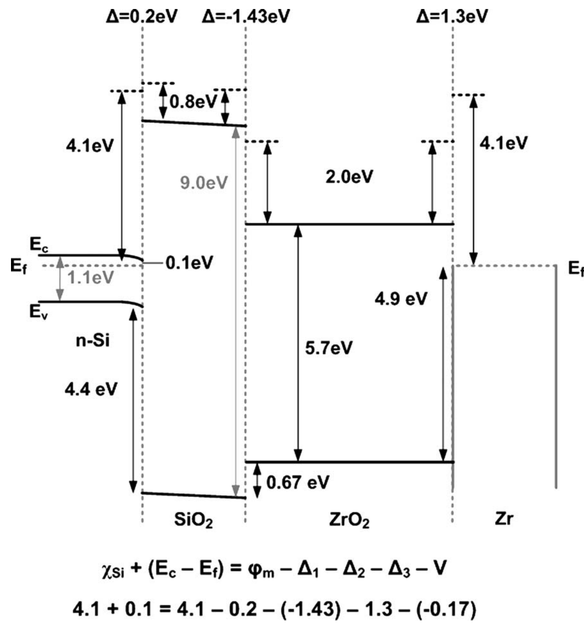

FIG. 10. A schematic band diagram for 1.0 nm Zr metal on 1.0 nm ZrO_2 on 0.5 nm SiO_2 on *n*-Si. The Zr work function of 4.1 eV, the oxide electron affinities, and the dipoles at each interface are indicated. Below is the balanced equation for the difference in the Si and Zr work functions including the dipole contribution from each interface and the potential across the dielectric layers.

underlying layers. The valence band spectrum displays emission extending to the Fermi energy, indicating metallic character. The metal work function can then be determined from the binding energy of the vacuum cutoff and the photon energy. The Zr metal work function is found to be $\Phi_M=21.2-17.1\pm0.14=4.1\pm0.14$ eV, which is similar to other reports.[20,21]

Figure 10 presents the final band alignment as deduced for this layered structure. The change in the interface dipole for the $Zr-ZrO_2$ interface is again determined from the measured work functions, electron affinities, and internal potential, and a value of $\Delta=1.3\pm0.4$ eV is determined. The Si work function is $4.1+0.3=4.4$ eV, which is slightly larger than the measured 4.1 eV work function of Zr. However, the results indicate the presence of an internal field causing downward band bending in the Si, a 0.17 V potential across the SiO_2, and a potential in the ZrO_2 layer that is below our detection limits. We expect that a potential due to a work function mismatch would be manifested as core level shifts in the high-κ layer as well as the SiO_2; however, the magnitude of the observed shifts should scale with the relative dielectric constants, meaning that the voltage drop across the ZrO_2 would be perhaps a factor of 5 smaller ($\kappa=20$) than that in SiO_2. The 0.17 V potential across the SiO_2 layer would correspond with a potential across the ZrO_2 of $\sim$0.033 V, well below our experimental sensitivity of $\pm$0.1 eV.

The structures studied here were prepared with e-beam evaporation techniques while technological implementation would most likely employ chemical vapor deposition (CVD) or atomic layer deposition (ALD) approaches. We would anticipate that the interface band offsets observed here would be independent of the deposition technique; however, the presence of internal fields is highly sensitive to defects in the films and could be significantly affected by the deposition process.

D. Band alignment and interface dipole effects

Our findings suggest that while the electron affinity model works well for predominantly covalent materials such as SiO_2 on Si ($\Delta=0.2$ eV), it is not well suited for more ionic materials such as ZrO_2 (e.g., the SiO_2-ZrO_2 system where $\Delta=-1.43$ eV). Similarly the Schottky-Mott model of metal-semiconductor interfaces fails to predict the ZrO_2-Zr interface band alignment where the deviation $\Delta=-1.3$ eV. Evidently, aligning vacuum levels across an interface is insufficient to predict the band alignments in the $Zr-ZrO_2-SiO_2-Si$ system.

Robertson and Mönch have extended the metal induced gap states (MIGS) model to include semiconductor-semiconductor and semiconductor-dielectric interfaces.[22,23] They have given this generalized model the more general name of interface induced gap states (IFIGS). Rather than using the surface vacuum level as the reference level, the IFIGS model utilizes the branch point of the surface states, also termed the charge neutrality level (CNL). The model presumes that every semiconductor and insulator material will exhibit surface states that are both valence- and conduction-band-like. The CNL defines the energy at which their character changes from valence- to conduction-band-like. The CNL is the highest occupied state in the gap, which is like a Fermi level of the intrinsic gap states.

The IFIGS model suggests that charge will transfer across a metal-semiconductor interface and tend to align the metal Fermi level and the semiconductor CNL. Similarly for a semiconductor-dielectric interface, charge will transfer and tend to align the CNLs. Another view is that the charge transfer across the interface is due to chemical bonding.[6] The charge that is transferred across these bonds changes the interface dipole and can alter the barrier height. The polarity of the bonds can then be related to the difference in the electronegativities of the two materials in contact.

Mönch has recently combined the physical IFIGS model and the chemical electronegativity approach to approximate the valence band offset of an ideal heterostructure with

$$\Delta E_V = \Phi^p_{\mathrm{bp},a} - \Phi^p_{\mathrm{bp},b} + D_X(X_a - X_b), \quad (6)$$

where Φ^p_{bp} is the branch-point energy of material a or b relative to the VBM. The values X_a and X_b are the corresponding electronegativities and D_X is a slope parameter determined by the density of states and the extension of the IFIGS at the branch point. In this approach insulators are considered as wide band gap semiconductors and Eq. (6) applies equally to dielectric-dielectric interfaces.

The Schottky barrier height for a semiconductor-metal interface is given by a similar equation

$$\Phi_{ms} = \Phi^p_{\mathrm{bp}} - S_X(X_m - X_s), \quad (7)$$

where Φ^p_{bp} is the branch point energy of the semiconductor, S_X is a slope parameter, and X_m and X_s are the electronega-

TABLE III. Tabulated values of the slope parameter ϕ_{VBO}, the branch-point energy Φ_{bp}, the Miedema electronegativity X, the optical dielectric constant ε_∞, and the slope parameter S_X.

Material	E_G (eV)	ϕ_{VBO} [a]	Φ_{bp} (eV)	X (Miedema)[b]	ε_∞ [c]	S_X (eV/Miedema)
Si	1.1	n/a	0.36[d]	4.70	12	n/a
SiO_2	9.0	1.23	3.99	6.42	2.25	0.74
ZrO_2	5.7	1.17	3.36	5.76	4.80	0.35
Zr	n/a	n/a	n/a	3.40	n/a	n/a

[a]See Ref. 23.
[b]See Ref. 24.
[c]See Ref. 25.
[d]See Ref. 4.

tivities of the metal and semiconductor, respectively. The slope parameter S_X is given by

$$S_X = \frac{0.86}{1 + 0.1(\varepsilon_\infty - 1)^2}, \tag{8}$$

where ε_∞ is the optical dielectric constant and the units of S_X are eV/Miedema electronegativity unit.

Mönch asserts that the electric-dipole term $D_X(X_a - X_b)$ from Eq. (6) can be neglected because the electronegativities of atoms constituting the group-IV semiconductors and the III–V, II–VI, and I–III–IV_2 compounds only differ by up to about 10%. Thus Eq. (6) reduces to simply the difference in the branch-point energies,

$$\Delta E_V = \Phi^p_{bp,a} - \Phi^p_{bp,b}. \tag{9}$$

Experimental results have indicated a linear dependence of the valence band offsets, ΔE_V, on the branch point energy Φ^p_{bp}. Consequently, Eq. (9) has been modified with an empirical slope parameter and becomes

$$\Delta E_V = \varphi_{VBO}[\Phi^p_{bp,a} - \Phi^p_{bp,b}], \tag{10}$$

where the slope parameter φ_{VBO} has been experimentally found to range between 1.14 and 1.23.

Contained in Table III are parameters for the materials of interest in this study. The Si branch-point energy is the value calculated by Tersoff[24] while the others are from Mönch.[23] Using the parameters in Table III along with Eqs. (8)–(10), the predicted band alignments can be determined. For comparison, the calculated and experimental results are listed in Table IV. It is important to note that the IFIGS model intrinsically accounts for the interface bonding and the effect of the interface dipole. Our approach is to compare the experimentally determined band offsets with the prediction of the IFIGS model. The observed difference in the vacuum levels (Δ) is then presented as a correction to the electron affinity or Shottky-Mott models.

Using the Tersoff value for the Si branch-point energy (0.36 eV) and the Mönch value for SiO_2 (3.99 eV) to calculate the valence band offset, we find that calculation (4.46 eV) and experiment (4.4 eV) differ by only 0.06 eV.

The branch-point energy predicted for ZrO_2 has ranged from 3.2 eV, as reported by Mönch,[23] to values of 3.3 or 3.6 eV from Robertson,[4] and Peacock and Robertson.[8] Taking the average of these values gives a branch-point energy of 3.36 eV above E_V. Using this value with Eq. (10) and the slope parameter of 1.17 as given by Mönch, the calculated offset for the SiO_2–ZrO_2 interface is 0.73 eV. This is essentially consistent with the experimental value of 0.67 eV.

To calculate the p-type barrier height for the ZrO_2–Zr interface Eq. (7) is used along with 3.36 eV as the branch-point energy and the Miedema electronegativities and slope parameter, as listed in Table III.[25] A p-type barrier of 4.03 eV is determined, which corresponds to an n-type barrier of 1.67 eV where a 5.7 eV band gap was used for ZrO_2. The calculated value is larger than the observed conduction band barrier of 0.8 eV and we consider possible sources of the deviation from the model. The branch-point energy of 3.36 eV gave a good agreement for the SiO_2–ZrO_2 interface so it is reasonable to presume that the value is appropriate. The slope parameter may be a source of error as its dependence on the optical dielectric constant has been empirically determined. Additionally, the optical dielectric constant from Robertson (Table I) may be inappropriate for a ZrO_2 thin film.[4] As an exercise we calculate the slope parameter from the observed Zr–ZrO_2 Schottky barrier of 0.8 eV and find that if S_X=0.65 (versus the calculated value of 0.35) the IFIGS model would be consistent with measurements.

TABLE IV. Calculated barrier heights from the IFIGS model, the electron affinity or Schottky-Mott (EA/SM) model, and a comparison with the measured values. The CBO values presume the band gaps, as listed in Table III.

Interface	IFIGS VBO	EA/SM VBO	Measured VBO	IFIGS CBO	EA/SM CBO	Measured CBO
Si–SiO_2	4.46	4.6	4.4±0.1	3.44	3.3	3.5±0.1
SiO_2–ZrO_2	0.73	2.1	0.67±0.24	2.57	1.2	2.63±0.24
ZrO_2–Zr	4.18	3.6	4.90±0.44	1.67	2.1	0.80±0.44

It is also likely that the simplistic view of the interface, with a well defined ZrO_2 on one side and Zr on the other, is unrealistic. It is probable that the deviation can be represented as a combination of a more complex interface structure and a correction to the Schottky pinning parameter.

An intriguing aspect of the band alignment is that the large changes of the interfaces dipole that exist at the ZrO_2 interfaces are opposite in sign and nearly equal in magnitude. The sum of the interface dipole changes across the entire gate stack nearly cancel, suggesting that an *I-V* measurement of this gate stack would nearly agree with the original Schottky-Mott model, while missing the large dipole effects in the band alignment of ZrO_2.

V. CONCLUSIONS

In this study *in situ* deposition and photoemission spectroscopy have been employed to characterize a potential metal oxide *n*-type semiconductor gate stack in a stepwise manner, determining the valence band offsets, vacuum levels, internal fields, and changes in band bending after each deposition step. The results from this sequential growth and characterization technique allow us to calculate, for each interface, the deviation of the electronic barrier heights as determined from the alignment of the material vacuum levels. This deviation, or change of the interface dipole, is thought to result from charge transfer across the interface. The observed band alignment has been compared to an interface-induced gap states model, as presented by Robertson and Mönch.[4,23] This model incorporates the predicted band structure and a dipole contribution due to the chemical potential across the interface. The IFIGS model provides an agreement with our results for both the $Si-SiO_2$ and the SiO_2-ZrO_2 interface. The discrepancy of the model and experiment for the ZrO_2-Zr interface may be attributable to a more refined value of the Schottky pinning parameter or to a more complex interface structure. Most interesting is the finding that across the completed gate stack, the sum of the interface dipole changes is nearly zero, suggesting that electrical measurements would find barrier heights reasonably close to those predicted by the Schottky-Mott model and would not be sensitive to variations at the individual interfaces or to the actual band alignment.

ACKNOWLEDGMENTS

This work is supported through the Semiconductor Research Corporation, NCSU Front End Process Center, Office of Naval Research, and the Air Force Office of Scientific Research.

[1] G. D. Wilk, R. M. Wallace, and J. M. Anthony, J. Appl. Phys. **89**, 5243 (2001).
[2] J. P. Chang, Y.-S. Lin, S. Berger, A. Kepten, R. Bloom, and S. Levy, J. Vac. Sci. Technol. B **19**, 2137 (2001).
[3] E. P. Gusev, E. Cartier, D. A. Buchanan, M. Gribelyuk, M. Copel, H. Okorn-Schmidt, and C. D'Emic, Microelectron. Eng. **59**, 341 (2001).
[4] J. Robertson, J. Vac. Sci. Technol. B **18**, 1785 (2000).
[5] Semiconductor Industry Association, *International Technology Roadmap for Semiconductors*, 2003 ed. (SEMATECH, Austin, TX, 2003).
[6] C. B. Duke and C. Mailhiot, J. Vac. Sci. Technol. B **3**, 1170 (1985).
[7] J. Bardeen, Phys. Rev. **71**, 717 (1947).
[8] P. W. Peacock and J. Robertson, J. Appl. Phys. **92**, 4712 (2002).
[9] W. Mönch, J. Appl. Phys. **80**, 5076 (1996).
[10] A. Fissel, J. Dabrowski, and H. J. Osten, J. Appl. Phys. **91**, 8986 (2002).
[11] C. C. Fulton, G. Lucovsky, and R. J. Nemanich, Appl. Phys. Lett. **84**, 580 (2004).
[12] J. R. Shallenberger, D. A. Cole, and S. W. Novak, J. Vac. Sci. Technol. A **17**, 1086 (1999).
[13] M. P. Seah and W. A. Dench, Surf. Interface Anal. **1**, 2 (1979).
[14] J. C. Ashley and C. J. Tung, Surf. Interface Anal. **4**, 52 (1982).
[15] C. Fulton, G. Lucovsky, and R. J. Nemanich, J. Vac. Sci. Technol. B **20**, 1726 (2002).
[16] A. C. Tuan, T. C. Kaspar, T. Droubay, J. W. Rogers, Jr., and S. A. Chambers, Appl. Phys. Lett. **83**, 3734 (2003).
[17] J. W. Keister, J. E. Rowe, J. J. Kolodziej, H. Niimi, T. E. Madey, and G. Lucovsky, J. Vac. Sci. Technol. B **17**, 1831 (1999).
[18] S. M. Sze, *VLSI Technology*, 2nd ed. (McGraw-Hill Book, New York, 1988).
[19] S. Miyazaki, M. Narasaki, M. Ogasawara, and M. Hirose, Solid-State Electron. **46**, 1679 (2002).
[20] H. B. Michaelson, IBM J. Res. Dev. **22**, 72 (1978).
[21] V. Misra, G. P. Heuss, and H. Zhong, Appl. Phys. Lett. **78**, 4166 (2001).
[22] J. Robertson, Eur. Phys. J.: Appl. Phys. **28**, 265 (2004).
[23] W. Mönch, Appl. Phys. Lett. **86**, 122101 (2005).
[24] J. Tersoff, Surf. Sci. **168**, 275 (1986).
[25] A. R. Miedema, P. F. de Chate, and F. R. de Boer, Physica B & C **100**, 1 (1980).